PROTEIN STRUCTURE REPORT

Intermolecular versus intramolecular interactions of the vinculin binding site 33 of talin

S. D. Yogesha,[1] A. Sharff,[2] G. Bricogne,[2] and T. Izard[1]*

[1]Cell Adhesion Laboratory, Department of Cancer Biology, The Scripps Research Institute, Jupiter, FL 33458
[2]Global Phasing Ltd, Sheraton House, Castle Park, Cambridge CB3 0AX, United Kingdom

Received 20 April 2011; Revised 24 May 2011; Accepted 25 May 2011
DOI: 10.1002/pro.671
Published online 6 June 2011 proteinscience.org

Abstract: The cytoskeletal proteins talin and vinculin are localized at cell-matrix junctions and are key regulators of cell signaling, adhesion, and migration. Talin couples integrins via its FERM domain to F-actin and is an important regulator of integrin activation and clustering. The 220 kDa talin rod domain comprises several four- and five-helix bundles that harbor amphipathic α-helical vinculin binding sites (VBSs). In its inactive state, the hydrophobic VBS residues involved in binding to vinculin are buried within these helix bundles, and the mechanical force emanating from bound integrin receptors is thought necessary for their release and binding to vinculin. The crystal structure of a four-helix bundle of talin that harbors one of these VBSs, coined VBS33, was recently determined. Here we report the crystal structure of VBS33 in complex with vinculin at 2 Å resolution. Notably, comparison of the apo and vinculin bound structures shows that intermolecular interactions of the VBS33 α-helix with vinculin are more extensive than the intramolecular interactions of the VBS33 within the talin four-helix bundle.

Keywords: cytoskeleton; crystallography; focal adhesion; protein–protein interactions

Introduction

Talin plays essential roles in focal adhesion assembly, where its *N*-terminal FERM (4.1/ezrin/radixin/moesin) domain binds to the cytoplasmic tails of β-integrin subunits to activate integrins.[1,2] Talin is a large (over 2500 residues) cytoskeletal protein and its atypical FERM domain links to a long, flexible 220 kDa rod domain.[3] The talin rod domain is comprised of 63 α-helices that appear to be arranged as a series of four- and five-helix bundle domains. Notably, many of these bundles harbor latent amphipathic α-helical vinculin binding sites (VBS) that can bind to and activate vinculin.[4] In its inactive state, these talin VBSs are buried within these bundles via hydrophobic interactions with other α-helices in the bundle. Mechanical force on talin emanating from integrin receptors is sufficient to unfurl helix bundles bearing these VBSs to allow their binding to vinculin.[5,6]

The cytoskeletal protein vinculin is a key regulator of focal adhesions[7] by linking talin to the actin

Abbreviations: ANL, Argonne National Laboratory; APS, advanced photon source; Å, Ångstrom; FAK, focal adhesion kinase; FERM, 4.1/ezrin/radixin/moesin; GST, glutathione S-transferase; IPTG, isopropyl-β-thio-galactoside; SER-CAT, southeast regional collaborative access team; TLS, translation, libration, and screw-motion; VBS, vinculin binding site; Vh1, vinculin head domain 1; Vt, vinculin tail.

Additional Supporting Information may be found in the online version of this article.

The coordinates have been deposited with the Protein Data Bank (PDB entry 3s90).

*Correspondence to: T. Izard, Cell Adhesion Laboratory, Department of Cancer Biology, The Scripps Research Institute, Jupiter, FL 33458. E-mail: mkernick@scripps.edu

Published by Wiley-Blackwell. © 2011 The Protein Society

cytoskeleton and recruiting many other proteins.[8] Vinculin was also shown to regulate the mechanical stress of the extracellular environment and to function as a mechano-coupling protein.[9] Our human full-length 117 kDa vinculin and 124 kDa metavinculin crystal structures[10–12] showed that the globular vinculin head (VH) domain is comprised of three seven-helix bundles (Vh1–Vh3) and a four-helix bundle (Vt2). A proline-rich hinge region links VH and to a five-helix bundle tail domain. Vinculin is held in its inactive state[13] via extensive hydrophobic interactions of the vinculin tail (Vt) domain with the *N*-terminal Vh1 domain.[10,11,14] We determined the first talin bound Vh1 structure which showed that talin activates vinculin by severing the head–tail interaction by helix bundle conversion whereby the α-helical VBS inserts into the Vh1 four-helix bundle domain.[14] Severing the head–tail interaction reveals masked binding sites for F-actin, thus completing and maintaining links of integrin receptors with the actin network at focal adhesions. Subsequently, several other crystal structures of Vh1 in complex with talin VBSs,[15–17] as well as the VBSs of α-actinin[18] and the *Shigella* invasin IpaA[19–21] have been determined which are all very similar, and all of these use nearly identical mechanism of vinculin activation by helix bundle conversion.

Crystal and NMR structures of several helix bundle domains of talin have been reported, including those harboring VBS1,[22] VBS2,[17] VBS3,[23] VBS33,[24] and VBS36.[24] In all of these structures, the hydrophobic VBSs are buried and this suggested a requirement of talin activation for high affinity binding to vinculin,[17,18,22] which was confirmed by atomic force experiments that unravel the helix bundles of talin (and α-actinin) to allow the binding of their VBSs to vinculin.[5] Notably, as seen for other VBSs, the VBS33 residues involved in binding vinculin are buried within a four-helix bundle domain, yet this bundle readily binds to vinculin.[24] Here, we report the crystal structure of VBS33 in complex with the vinculin Vh1 domain at 2 Å resolution. Superposition of the VBS33 α-helix in its apo talin structure onto its vinculin bound state reveals far greater intermolecular interactions of VBS33 when bound to vinculin than intramolecular interactions of VBS33 within the talin four-helix bundle domain.

Results

The crystal structure of vinculin in complex with the talin VBS33

We determined the Vh1:VBS33 crystal structure to 2 Å resolution by molecular replacement using the Vh1 domain of the Vh1:IpaA-VBS structure[20] (Protein Data Bank (PDB) entry 2ibf) as the search model. The space group was *P*1 with two heterodimers in the asymmetric unit. Electron density was not visible for Vh1 residues 1–2 and 251–252 (chain A), and VBS33 residues 1512–1519 (chains C and D) and 1546 (chain D) due to disorder. VBS33 was traced into the *Fo–Fc* electron density map where Phe-1535 and Lys-1541 provided unambiguous markers for the tracing and directionality. The final crystallographic and free *R*-factors are 0.19 and 0.21, respectively. The quality of the model was assessed using both PROCHECK[25] and MolProbity[26] and 97% of all residues lie in most favored regions of the Ramachandran plot with the remaining 3% residues in additional allowed regions. The clashscore reported by MolProbity was in the 99th percentile, and the overall MolProbity score for the model is in the 98th percentile. Refinement statistics are provided in Table I.

VBS33 binds to vinculin in a fashion that is very similar to that seen in the six other crystal structures of talin VBSs in complex with Vh1 (Supporting Information, Figure S1) with highest

Table I. *X-ray Data Reduction and Crystallographic Refinement Statistics*

(*A*) X-ray data reduction statistics	
Space group	*P*1
Unit cell dimensions	
a, b, c	48.83 Å, 61.18 Å, 71.42 Å
α, β, γ	83.27°, 79.05°, 70.01°
Resolution	70.01 Å – 1.97 Å
(last shell)	(1.98 Å – 1.97 Å)
Total measurements	141,191
Number of unique reflections	51,772
(last shell)	(510)
Wavelength	1 Å
R-merge[a] (last shell)	0.043 (0.533)
I/σ(I) (last shell)	14.2 (2.3)
Completeness (last shell)	0.967 (0.959)
Redundancy (last shell)	0.028 (0.029)
(*B*) Crystallographic refinement statistics	
Resolution	70.01 Å – 1.97 Å
(last shell)	(1.98 Å – 1.97 Å)
No. of reflections (working set)	49,115
No. of reflections (test set)	2,625
R-factor[b] (last shell)	0.186 (0.218)
R-free[c] (last shell)	0.21 (0.233)
No. of amino acid residues	544
No. of atoms	4,694
No. of solvent molecules	406
Average B-factor	
Protein	50.8 Å^2
Solvent	54.3 Å^2
R.m.s.d. from ideal geometry	
Bond lengths	0.01 Å
Bond angles	0.97°

[a] $R-\text{merge} = \sum_{\text{hkl}}\sum_{i}|I_i(\text{hkl}) - \overline{I(\text{hkl})}|/\sum_{\text{hkl}}\sum_{i}I_i(\text{hkl})$

[b] $R-\text{factor} = \sum_{\text{hkl}}||F_{\text{obs}}(\text{hkl})| - |F_{\text{calc}}(\text{hkl})||\sum_{\text{hkl}}|F_{\text{obs}}(\text{hkl})|,$

where $<|F_{\text{calc}}|>$ denotes the expectation of $|F_{\text{calc}}(\text{hkl})|$ used in defining the likelihood refinement target.

[c] The free *R*-factor is a cross-validation residual calculated by using about 5% reflections, which were randomly chosen and excluded from the refinement.

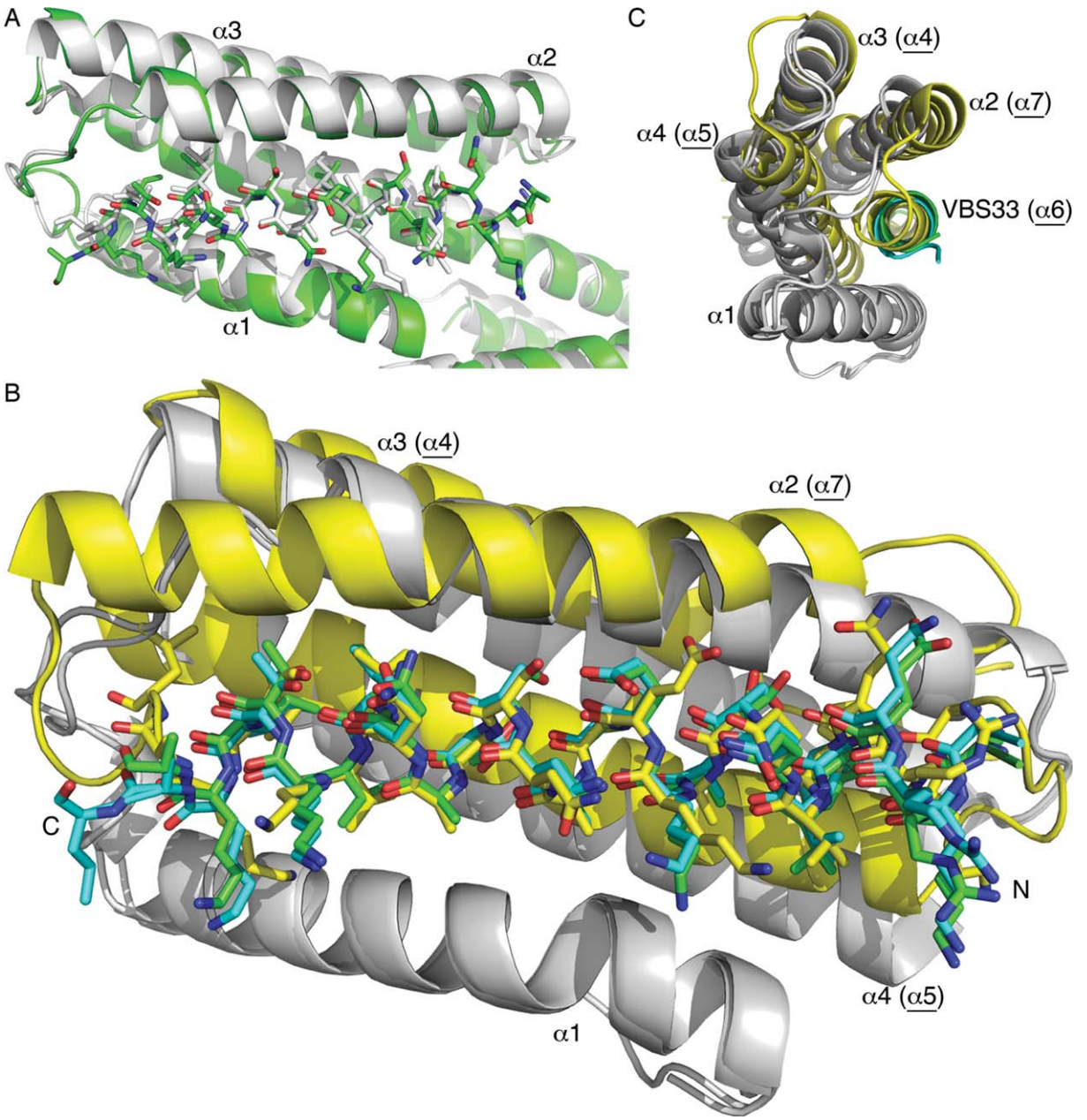

Figure 1. The talin domain harboring VBS33 unfurls upon binding to vinculin. (A) Zoomed view of the superposition of the Vh1:VBS33 (shown in green) onto the most similar structure Vh1:VBS58 (gray). Vinculin is shown as a cartoon and the respective VBSs are shown in ball-and-stick representation. (B, C) Cartoon drawing of human vinculin Vh1 domain (gray) in complex with VBS33 shown in cyan and green ball-and-stick representation for the two heterodimers in the asymmetric unit, respectively. Human VBS33 (residues 1522–1544) in its Vh1-bound state is superimposed onto the apo structure of the four-helix bundle domain of talin that harbors the VBS33 (residues 1457–1585; shown in yellow; PDB entry 2x0c) from *Mus Musculus* with *r.m.s.d*. of 1 Å for 156 atoms. This superposition places α2 of Vh1 (labeled; residues 40–62) similarly to α7 in talin (underlined; residues 1551–1577), α3 of Vh1 (residues 68–95) similarly to α4 in talin (underlined; residues 1464–1483), and α4 of Vh1 (residues 102–129) similarly to α5 in talin (underlined; residues 1487–1514). Panels (B) and (C) are orthogonal views.

Z-scores[27] for the Vh1:VBS58 (PDB entry 1zw2)[16] [Figure 1(A)]. All seven Vh1:VBS crystal structures[15–17] have the VBS inserted into the amino-terminal four-helix Vh1 subdomain by helix bundle conversion.[14] Further, in all seven Vh1:VBS crystal structures, the talin VBS α-helix is parallel to Vh1 α-helix α1 and antiparallel to α-helix α2. In addition, structure-based sequence alignment revealed that similar VBS residues are involved in binding to the same region of vinculin. Specifically, the 21 core residues of VBS1, VBS2, VBS11, VBS33, VBS36, and VBS58 align with those of VBS3 with *r.m.s.d*. ranging from 0.5 Å to 1.1 Å. Notably, the central core shows almost identical backbone conformation for all seven talin VBSs while the termini show more relative movements (Supporting Information, Figure S1).

The *N*-terminal vinculin four-helix bundle domain displays very similar conformations when aligning all of the VBSs of talin, yet Vh1:VBS33 is most similar to Vh1:VBS58.

The two heterodimers in the asymmetric unit are very similar and can be superimposed with *r.m.s.d.* of 0.6 Å for 1901 atoms. The largest differences, of over 5 Å, are seen furthest away from the VBS, in the loop region between the last two Vh1 α-helices, and these are due to crystal contacts. The α1–α2 loop that stretches over VBS33 and is often disordered in other Vh1:VBS crystal structures also displays slightly different conformations.

Distinct intermolecular versus intramolecular VBS33 interactions

The crystal structure of the talin domain that harbors VBS33 was recently determined to 2 Å resolution.[24] In talin, the domain harboring VBS33 is a four-helix bundle (with α-helices α4, α5, α6, and α7) that is inserted in a linker region after the third α-helix of a five-helix bundle domain (having helices α1, α2, α3, α8, and α9). The VBS33 α-helix is the sixth α-helix (α6) of the inserted four-helix bundle domain. This structure allowed us to examine the different environments of VBS33 when in its apo conformation *versus* its vinculin bound state [Figure 1(B,C); Supporting Information, Figure S2]. In its vinculin bound state, VBS33 is in contact with all four α-helices, while in the talin four-helix bundle VBS33 interacts with only two α-helices. Nevertheless, the native environment of VBS33 is similar to its vinculin-bound state as the directionality of structurally equivalent α-helices (VBS33, α2, α3, and α4) is the same as that in the talin four-helix bundle (α6, α7, α4, and α5) [Figure 1(C)].

Interestingly, the talin VBS33 (residues 1522–1545) engages in fewer interactions within the talin four-helix bundle versus when bound to the vinculin Vh1 domain [Figure 1(B,C); Supporting Information, Figure S2]. Specifically, 12 VBS33 residues are in contact with 15 talin residues, while 24 vinculin Vh1 residues interact with 18 VBS33 residues (Supporting Information, Figure S2). Indeed, with the exception of talin residues Lys-1522, Phe-1525, and Thr-1542, all other VBS33 residues engage in more contacts with vinculin residues than they do with talin residues. This trend is seen for both hydrophobic and polar interactions, where for example only four polar interactions are manifest in the talin four-helix bundle structure *versus* six in the Vh1:VBS33 structure. These findings are also consistent with an increase of over 20% in buried solvent accessible surface area, where there is ~1130 Å^2 buried in the Vh1:VBS33 complex compared to ~900 Å^2 in the talin four-helix bundle structure when considering just the α-helices. They are also concordant with a reduced melting temperature (T_m = 42 °C)[24] of the four-helix bundle domain that harbors VBS33 compared to other talin bundles (T_m = 53.9 °C to 74.2°C)[28,29] and a clear negative correlation between the stability of the talin helix bundle and its ability to bind to vinculin has been established.[22] Nevertheless, the shape complementarity[30] is similar in both cases (0.71 for VBS33 within the talin four-helix bundle and 0.68 for VBS33 in the Vh1:VBS33 complex).

Discussion

The crystal structure of VBS33 in complex with vinculin resembles that of other talin VBS structures in complex with vinculin, yet a detailed comparison with its unbound structure reveals important differences for binding to and activating vinculin. Specifically, the data establish that VBS33 engages in more interactions when bound to vinculin versus in its unbound four-helix bundle, which is not the case for two other talin four-helix bundle domains, which harbor VBS11 or VBS2.[17]

As seen for other VBSs,[17,22,31] the VBS33[24] residues involved in vinculin binding are buried in the unbound four-helix bundle structure, confirming that talin needs to be activated to expose this cryptic VBS33 binding site to allow binding to vinculin.[5] Indeed, while the VBS33 four-helix bundle domain readily binds to vinculin in solution, a larger portion harboring both the five- and four-helix bundles of talin binds poorly to vinculin.[24]

Four structures of talin five-helix bundle domains that contain a VBS (VBS1, PDB entry 1sj7; VBS3, 2kvp; VBS36, 2x0c; and VBS58, 2jsw) have been reported, and in these cases the VBS is the second (in VBS58), the fourth (in VBS1 and VBS33), or the fifth (in VBS3) α-helix of the corresponding five-helix bundle domain. Thus, the environments of the VBSs in their respective bundles are quite distinct, especially since these five-helix bundle domains have distinct topologies.[22,24,31] On the contrary, the structures of the three known talin four-helix bundles that harbor VBSs are more similar, even though here as well the location of the VBS varies, where the VBS is the third (in VBS11[17] and VBS33[24]) or fourth (in VBS2[17]) α-helix of the corresponding four-helix bundle. Furthermore, VBS2 and VBS11 reside in the same four-helix talin bundle domain. Indeed, VBS33 appears to be the only VBS of talin that has more interactions with vinculin than in its unbound bundle-buried location. These findings might have implications and consequences on vinculin activation by talin and a special role for VBS33.

Materials and Methods

Cloning, protein expression and purification

The vinculin Vh1 domain (residues 1–252) was cloned into pET-24b (Novagen) using the *NdeI* and

XhoI restriction sites; this adds an additional methionine at the *N*-terminus that is not part of vinculin. Various lengths of VBS33 (residues 1518–1546, 1520–1544, 1512–1552, and 1512–1546) were cloned into pGEX-6P-1 (GE Lifesciences) using the *BamH1* and *EcoR1* sites to obtain GST-VBS33 having a PreScission protease cleavage site, resulting in additional Gly-Pro-Leu-Gly-Ser residues at the *N*-terminus that are not part of talin. All constructs were verified by sequencing.

Plasmids carrying GST-VBS33 and Vh1 were cotransformed into *Escherichia coli* BL21(DE3) (Invitrogen) and selected with appropriate antibiotics. Colonies were tested for expression of both proteins and inoculated in 30 ml Luria-Bertan (LB) medium and grown at 37 °C with antibiotics for overnight, inoculated into 1 L LB medium and grown for 4 h at 37 °C, and induced with 0.5 mM IPTG at 25 °C overnight. Pelleted cells were resuspended in tris buffered saline (TBS) buffer (20 mM Tris, 150 mM NaCl, pH 8), frozen at −80 °C, thawed on ice, lysed by sonication in 100 ml TBS in presence of one complete Mini (Roche) protease inhibitor cocktail tablet and lysates were centrifuged at 95,834 × *g* (35,000 *r.p.m*. using a Ti45 rotor) for 30 min. The filtered lysate was loaded on to a TBS equilibrated GST FF 16/20 affinity chromatography column and eluted with 10 mM reduced glutathione in TBS. The peak fractions were pooled according to sodium dodecyl sulfate polyacrylamide gel electrophoresis (SDS-PAGE) and subjected to PreScission protease (1 U/mg of protein) cleavage by dialysis in 50 mM Tris, 150 mM NaCl, 1 mM DTT, and 1 mM EDTA for 1 day at 4 °C. After confirming cleavage by SDS-PAGE, excess GST and uncleaved GST-VBS33 were removed by applying twice over a GST column. The pooled protein was concentrated and loaded onto a Superdex 75 size exclusion chromatography column pre-equilibrated with TBS. The peak fractions were analyzed to confirm the presence of both proteins. The Vh1:VBS33 complex was concentrated to 10 mg/ml. All chromatography columns are from GE Life Sciences.

Vh1:VBS33 crystallization

Crystallization screens at two temperatures resulted in two conditions (0.1 M sodium cacodylate, pH 5.5, 25% PEG 4000; or 0.1 M sodium acetate, pH 5, 1 M ammonium sulphate) that produced crystals of Vh1:VBS33 (talin residues 1520–1544 and 1518–1546) that diffracted to about 6 Å to 8 Å Bragg spacings. About one in five crystals (grown from a reservoir of 0.1 M sodium cacodylate, pH 6.2, 20% PEG 4000) diffracted to 2.5 Å to 3 Å Bragg spacings at the Advanced photon source (APS), Argonne National Laboratory (ANL), SER-CAT BM-22 beam line but the diffraction was anisotropic and suggested twinning. The longer VBS33s (residues 1512–1552 or 1512–1546) in complex with Vh1 resulted in single crystals grown by hanging drop vapor diffusion at 4 °C with a reservoir solution of 0.1 M citrate 5.3, 15% (w/v) PEG 10 K, and 1.5% (v/v) dioxane. The crystals were frozen in paratone oil. Best diffraction was obtained from VBS33 residues 1512–1546 in complex with Vh1.

X-ray diffraction data collection, reduction, structure determination, and crystallographic refinement

X-ray diffraction data of Vh1:VBS33 were obtained to 2 Å Bragg spacings at the APS, ANL, SER-CAT BM-22 beam line, and processed using autoProc[32] utilizing XDS[33] as the data reduction engine. The crystals belong to space group *P*1 (a = 48.83 Å, b = 61.18 Å, c = 71.42 Å, α = 48.83°, β = 61.18°, and γ = 71.42°) with two heterodimers in the asymmetric unit resulting in a solvent content of 0.65 and a Matthews coefficient of 3.51 Å^3/Da.[34] The data collection statistics are provided in Table I.

Phases were obtained by molecular replacement using the CCP4 program MOLREP[35] and the Vh1 domain of the Vh1:IpaA-VBS structure[20] (PDB entry 2ibf) as the search model. Crystallographic refinement was performed with autoBUSTER[36] with extensive model building using COOT.[37] The final rounds of the refinement applied translation, libration, and screw-motion (TLS) in autoBUSTER. TLS groups were obtained by the TLSMD server.[38]

Acknowledgments

We are indebted to our colleagues at Scripps Florida: John Cleveland for discussions and critical review of the manuscript, Zhen Wu and Philippe Bois for sequencing, and Philippe Bois and Rangarajan Erumbi for fruitful discussions. Finally, we are grateful to the staff at the APS, SER-CAT, for synchrotron support. TI is supported by grants from the National Institutes of Health and by start-up funds provided to Scripps Florida from the State of Florida. SDY is a fellow of the Department of Defense. This is publication no. 21234 from the Scripps Research Institute.

References

1. Moulder GL, Huang MM, Waterston RH, Barstead RJ (1996) Talin requires β-integrin, but not vinculin, for its assembly into focal adhesion-like structures in the nematode Caenorhabditis elegans. Mol Biol Cell 7:1181–1193.
2. Critchley DR, Holt MR, Barry ST, Priddle H, Hemmings L, Norman J (1999) Integrin-mediated cell adhesion: the cytoskeletal connection. Biochem Soc Symp 65:79–99.
3. Hemmings L, Rees DJ, Ohanian V, Bolton SJ, Gilmore AP, Patel B, Priddle H, Trevithick JE, Hynes RO, Critchley DR (1996) Talin contains three actin-binding sites each of which is adjacent to a vinculin-binding site. J Cell Sci 109:2715–2726.
4. Bois PR, O'Hara BP, Nietlispach D, Kirkpatrick J, Izard T (2006) The vinculin binding sites of talin and α-actinin are sufficient to activate vinculin. J Biol Chem 281:7228–7236.
5. del Rio A, Perez-Jimenez R, Liu R, Roca-Cusachs P, Fernandez JM, Sheetz MP (2009) Stretching single

talin rod molecules activates vinculin binding. Science 323:638–641.
6. Lee SE, Kamm RD, Mofrad MR (2007) Force-induced activation of talin and its possible role in focal adhesion mechanotransduction. J Biomech 40:2096–2106.
7. Jockusch BM, Rudiger M (1996) Crosstalk between cell adhesion molecules: vinculin as a paradigm for regulation by conformation. Trends Cell Biol 6:311–315.
8. Gilmore AP, Burridge K (1996) Regulation of vinculin binding to talin and actin by phosphatidyl-inositol-4–5-bisphosphate. Nature 381:531–535.
9. Mierke CT, Kollmannsberger P, Zitterbart DP, Smith J, Fabry B, Goldmann WH (2008) Mechano-coupling and regulation of contractility by the vinculin tail domain. Biophys J 94:661–670.
10. Rangarajan ES, Lee JH, Yogesha SD, Izard T (2010) A helix replacement mechanism directs metavinculin functions. PLoS ONE 5:e10679.
11. Borgon RA, Vonrhein C, Bricogne G, Bois PR, Izard T (2004) Crystal structure of human vinculin. Structure 12:1189–1197.
12. Rangarajan ES, Izard T (2010) Improving the diffraction of full-length human selenomethionyl metavinculin crystals by streak-seeding. Acta Crystallogr F 66:1617–1620.
13. Johnson RP, Craig SW (1994) An intramolecular association between the head and tail domains of vinculin modulates talin binding. J Biol Chem 269: 12611–12619.
14. Izard T, Evans G, Borgon RA, Rush CL, Bricogne G, Bois PR (2004) Vinculin activation by talin through helical bundle conversion. Nature 427:171–175.
15. Izard T, Vonrhein C (2004) Structural basis for amplifying vinculin activation by talin. J Biol Chem 279: 27667–27678.
16. Gingras AR, Ziegler WH, Frank R, Roberts GC, Critchley DR, Emsley J (2005) Mapping and consensus sequence identification for multiple vinculin binding sites within the talin rod. J Biol Chem 280:37217–37224.
17. Fillingham I, Gingras AR, Papagrigoriou E, Patel B, Emsley J, Critchley DR, Roberts GC, Barsukov IL (2005) A vinculin binding domain from the talin rod unfolds to form a complex with the vinculin head. Structure 13:65–74.
18. Bois PR, Borgon RA, Vonrhein C, Izard T (2005) Structural dynamics of α-actinin-vinculin interactions. Mol Cell Biol 25:6112–6122.
19. Izard T, Tran Van Nhieu G, Bois PR (2006) *Shigella* applies molecular mimicry to subvert vinculin and invade host cells. J Cell Biol 175:465–475.
20. Tran Van Nhieu G, Izard T (2007) Vinculin binding in its closed conformation by a helix addition mechanism. EMBO J 26:4588–4596.
21. Park H, Valencia-Gallardo C, Sharff A, Tran Van Nhieu G, Izard T (2011) A novel Vinculin binding site of the IpaA invasin of *Shigella*. J Biol Chem Apr 27. [Epub ahead of print].
22. Papagrigoriou E, Gingras AR, Barsukov IL, Bate N, Fillingham IJ, Patel B, Frank R, Ziegler WH, Roberts GC, Critchley DR, Emsley J (2004) Activation of a vinculin-binding site in the talin rod involves rearrangement of a five-helix bundle. EMBO J 23:2942–2951.
23. Gingras AR, Vogel KP, Steinhoff HJ, Ziegler WH, Patel B, Emsley J, Critchley DR, Roberts GC, Barsukov IL (2006) Structural and dynamic characterization of a vinculin binding site in the talin rod. Biochemistry 45: 1805–1817.
24. Gingras AR, Bate N, Goult BT, Patel B, Kopp PM, Emsley J, Barsukov IL, Roberts GC, Critchley DR (2010) Central region of talin has a unique fold that binds vinculin and actin. J Biol Chem 285:29577–29587.
25. Laskowski R, MacArthur MW, Thornton JM (1993) PROCHECK: a program to check the stereochemicai quality of protein structures. J Appl Cryst 26:283–291.
26. Chen VB, Arendall WB, 3rd, Headd JJ, Keedy DA, Immormino RM, Kapral GJ, Murray LW, Richardson JS, Richardson DC (2010) MolProbity: all-atom structure validation for macromolecular crystallography. Acta Crystallogr D Biol Crystallogr 66:12–21.
27. Holm L, Rosenstrom P (2010) Dali server: conservation mapping in 3D. Nucleic Acids Res 38:W545–W549.
28. Patel B, Gingras AR, Bobkov AA, Fujimoto LM, Zhang M, Liddington RC, Mazzeo D, Emsley J, Roberts GC, Barsukov IL, Critchley DR (2006) The activity of the vinculin binding sites in talin is influenced by the stability of the helical bundles that make up the talin rod. J Biol Chem 281:7458–7467.
29. Gingras AR, Ziegler WH, Bobkov AA, Joyce MG, Fasci D, Himmel M, Rothemund S, Ritter A, Grossmann JG, Patel B, Bate N, Goult BT, Emsley J, Barsukov IL, Roberts GC, Liddington RC, Ginsberg MH, Critchley DR (2009) Structural determinants of integrin binding to the talin rod. J Biol Chem 284:8866–8876.
30. Lawrence MC, Colman PM (1993) Shape complementarity at protein/protein interfaces. J Mol Biol 234: 946–950.
31. Gingras AR, Bate N, Goult BT, Hazelwood L, Canestrelli I, Grossmann JG, Liu H, Putz NS, Roberts GC, Volkmann N, Hanein D, Barsukov IL, Critchley DR (2008) The structure of the C-terminal actin-binding domain of talin. EMBO J 27:458–469.
32. Vonrhein C, Flensburg C, Keller P, Sharff A, Smart O, Paciorek W, T. W, Bricogne G (2011) Data processing and analysis with the autoPROC toolbox. Acta Crystallogr D Biol Crystallogr 67:293–292.
33. Kabsch W (2010) XDS. Acta Crystallogr D Biol Crystallogr 66:125–132.
34. Matthews BW (1968) Solvent content of protein crystals. J Mol Biol 33:491–497.
35. Vagin A, Teplyakov A (1997) MOLREP: an automated program for molecular replacement. J Appl Crystallogr 30:1022–1025.
36. Bricogne G, Blanc E, Brandl M, Flensburg C, Keller P, Paciorek P, Roversi P, Sharff A, Smart O, Vonrhein C, Womack T (2010) BUSTER version 2.9. Cambridge, United Kingdom: Global Phasing Ltd.
37. Emsley P, Cowtan K (2004) Coot: model-building tools for molecular graphics. Acta Crystallogr D Biol Crystallogr 60:2126–2132.
38. Painter J, Merritt EA (2006) Optimal description of a protein structure in terms of multiple groups undergoing TLS motion. Acta Crystallogr D Biol Crystallogr 62:439–450.